



# Application of 1D and 2D hydrodynamic modeling to study glacial lake outburst flood (GLOF) and its impact on a hydropower station in Central Himalaya

Ashim Sattar<sup>1,2</sup> · Ajanta Goswami<sup>2</sup> · Anil V. Kulkarni<sup>3</sup>

Received: 16 August 2018 / Accepted: 1 July 2019 / Published online: 6 July 2019  
© Springer Nature B.V. 2019

## Abstract

The existence of numerous lakes in the higher reaches of the Himalaya makes it a potential natural hazard as it imposes a risk of glacial lake outburst flood (GLOF), which can cause great loss of life and infrastructure in the downstream regions. Hydrodynamic modeling of a natural earth-dam failure and hydraulic routing of the breach hydrograph allow us to characterize the flow behavior of a potential flood along a given flow channel. In the present study, the flow hydraulics of a potential GLOF generated due to the moraine failure of the Satopanth lake located in the Alaknanda basin is analyzed using one-dimensional and two-dimensional hydrodynamic computations. Field measurements and mapping were carried out at the lake site and along the valley using high-resolution DGPS points. The parameters of Manning's roughness coefficient and terrain elevation were derived using satellite-based raster, the accuracy of which is verified using field data. The volume of the lake is calculated using area-based scaling method. Unsteady flood routing of the dam-break outflow hydrograph is performed along the flow channel to compute hydraulic parameters of peak discharge, water depth, flow velocity, inundation and stream power at a hydropower dam site located 28 km downstream of the lake. Assuming the potential GLOF event occurs contemporaneously with a 100-year return period flood, unsteady hydraulic routing of the combined flood discharge is performed to evaluate its impact on the hydropower dam. The potential GLOF resulted in a peak discharge of  $\sim 2600 \text{ m}^3 \text{ s}^{-1}$  at the dam site which arrived 38 min after the initiation of the moraine-failure event. The temporal characteristics of the flood wave analyzed using 2D unsteady simulations revealed maximum inundation depth and flow velocity of 7.12 m and  $7.6 \text{ ms}^{-1}$ , respectively, at the dam site. Assuming that the control gates of the dam remain closed, water depth increases at a rate of 4.5 m per minute and overflows the dam approximately 4 min after the flood wave arrival.

**Keywords** Glacial lake outburst flood (GLOF) · 1D and 2D hydrodynamic modeling · Mountain hazard · Himalaya · HEC-RAS · Hydropower station

---

✉ Ashim Sattar  
ashim.sattar@gmail.com

<sup>1</sup> NIIT University, Rajasthan 301705, India

<sup>2</sup> Indian Institute of Technology Roorkee, Roorkee 247667, India

<sup>3</sup> Indian Institute of Science, Bangalore 560012, India

## 1 Introduction

Glacier retreat driven by climate change has led to the formation of numerous glacial lakes (Komori 2008; Gardelle et al. 2011). The formation of these lakes is considered to be emerging threat, as catastrophic failure of these lakes may cause great damage to the low-lying communities and infrastructure (Lliboutry et al. 1977; Haeberli 1983; Carey 2005; Mergili and Scheider 2011; Stoffel and Huggel 2012; Sattar et al. 2019). Over the past decade, high-altitude lakes in the Himalaya have shown significant growth in their size and number, and with this the ever threatening hazard of glacial lake outburst flood (GLOF) has increased manifold (Richardson and Reynolds 2000; Ageta et al. 2000; Mool et al. 2001; Quincey et al. 2007; Ives et al. 2010; Gardelle et al. 2011; Nie et al. 2013; Wang et al. 2015). These changes occur due to a general trend of glacier recession, remarkably observed in the Hindu Kush Himalaya (Kulkarni et al. 2007; Bolch et al. 2012). Moraine-dammed lakes are formed when glacier meltwater is trapped between the end moraine and the glacier snout (Westoby et al. 2014). However, such lakes may also form when glacier- or snowmelt water is blocked by a lateral moraine. The lakes are most commonly called as blocked lakes (Raj and Kumar 2016). The increase in the volume of these lakes may lead to percolation of the water into the moraine, thereby affecting the stability of the dam (Clague and Evans 2000). In the Himalaya, intense cloudburst events may also contribute to the total lake volume, which may exert pressure on damming material and eventually lead to a failure event (Worni et al. 2012). The severity of a GLOF depends on the volume of water released during the failure event and also the terrain characteristics (Westoby et al. 2014). These lake-failure events are most often triggered by snow or rock avalanche, glacier calving or seismic activity (Richardson and Reynolds 2000; Westoby et al. 2014).

India is a subtropical country, in which 80% annual precipitation is received in the monsoon season from June to September every year (Ghosh et al. 2009). Spatial distribution of the rainfall shows high precipitation along the Himalayan arc (Bookhagen and Burbank 2006). Trend analysis of the annual occurrences of rainfall shows a significant increase in the high to extremely high rainfall occurrences, especially over Uttarakhand and Himachal Pradesh (Ghosh et al. 2009). It is also reported that rainfall over the northern part of India may migrate rapidly toward the high-altitude regions due to excessive moisture convergence into the low-pressure pockets (Pattanaik et al. 2015). These rainfall events can have a significant impact on the Himalayan cryosphere. Rain on snow accelerates the melting process and can cause downstream flooding (Heeswijk et al. 1996). The formation of new high-altitude lakes and an increase in the volume of the existing lakes are other significant effects of rainfall over the high-altitude regions in the Himalaya (Komori 2008). The water accumulated during heavy rainfall can significantly increase the pre-existing volume of a glacial lake, thereby exerting additional pressure on the embankment and thus could affect the integrity of the moraine (Westoby et al. 2014). A sudden increase in the lake volume may initiate overtopping flows, leading to the formation of an eventual breach (Clague and Evans 2000). Several GLOF events have been reported in the Himalaya (Richardson and Reynolds 2000; Ives et al. 2010), of which forty-seven has been documented so far (Emmer 2018). One such major event was the Kedarnath disaster, June 16–17, 2013, in which a cloudburst event and the failure of Chorabari lake led to over 6000 human fatalities and caused great damage to the downstream infrastructure (Dobhal et al. 2013; Ray et al. 2016; Allen et al. 2016). The Chorabari lake was a moderately small-sized seasonal glacial lake blocked by the western lateral moraine of the Chorabari glacier, mostly fed by snowmelt and rainfall runoff. Following the 2013 event, Uttarakhand Space Application

Centre (USAC) revealed satellite images showing the existence and growth of another lake called the Satopanth lake, located 26 km east of Chorabari glacier. The Satopanth lake has a very similar geological and geomorphologic setting as that of the Chorabari lake. Worni et al. (2012) performed a risk assessment of the glacial lakes in the Himalaya in which 93 glacial lakes including the Satopanth lake were reported to be potentially critical as it presents GLOF risk to the downstream regions. GLOF risk assessment became much necessary scrutiny for the state, following the flood event of 2013 that devastated parts of Uttarakhand.

A large number of hydroelectric power plants (HEP) were reported to have experienced great damage in the 2013 cloudburst and GLOF event (Das 2013). The 400 MW Jaypee (JP) Vishnuprayag HEP, located 28 km downstream of the Satopanth lake, was one of the affected HEP during the 2013 cloudburst event. Due to the fact that a number of glacial lakes exist within the limits of the Vishnuprayag HEP catchment, GLOF risk assessment for this hydropower station becomes very vital. Assuming that extreme rainfall events may occur contemporaneously with a catastrophic glacial lake failure within the catchment of the Vishnuprayag hydropower dam (similar to the 2013 event), the present study evaluates the hazard potential of a lake outburst combined with an extreme precipitation event and assesses its impact on the HEP.

So far, one-dimensional hydrodynamic models have been used popularly to understand GLOF waves in the Himalaya (Jain et al. 2012; Thakur et al. 2016). Very few studies have employed two-dimensional models to understand the hydraulic flow behavior of these events (Alho and Juha 2008; Osti and Egashira 2009; Worni et al. 2012; Sattar et al. 2019). This study incorporates (1) growth assessment of the Satopanth lake using multi-temporal satellite imagery, (2) field investigation of the lake and the associated valley, (3) hydrodynamic modeling to assess the hazard potential of Satopanth lake on the nearest hydropower station based on one-dimensional, two-dimensional models and ground data and (4) analysis of the potential GLOF impact of the Satopanth lake coupled with a 100-year return period flood event. The present study is an integration of remote sensing and field methods to evaluate the potential hazard of the Satopanth lake. The details of the remotely sensed and field datasets employed in the present study are given in Sect. 3. Hydrodynamic modeling to characterize a potential GLOF event is carried out using 1D and 2D hydraulic models, the methodology of which is explained in Sect. 4. Here, we model a potential GLOF event of the Satopanth lake in combination with a 100-year return period flood (Sect. 4.3.1). Section 5 presents the modeled hydraulic characteristics like peak flood, water depth, flow velocity, stream power and inundation of the potential flood wave.

## 2 Study area

The present study is carried out in the Alaknanda basin located in the state of Uttarakhand, Central Himalaya. The basin is mainly drained by two major glacier-fed rivers, namely Alaknanda and the Bhagirathi. The upper and the lower bounds of the catchment lie between latitude 30°15'22"N to 31°14'00"E and longitude 79°11'00"N and 80°28'00"E with a total area of 6385 km<sup>2</sup>. The Alaknanda river originates from the Satopanth and the Bhagirath Kharak glaciers and flows as Saraswati in the sub-watershed until it joins the Dhauliganga tributary at Vishnuprayag. The presence of a potentially critical lake (Satopanth) (Worni et al. 2012) upstream of a hydroelectric power plant (HEP) located over the Alaknanda mainstream at Vishnuprayag, Central Himalaya, bounds us to study the impact

of a potential GLOF event on the JP HEP. The Satopanth lake ( $30^{\circ}44'37''\text{N}$ ,  $79^{\circ}21'25''\text{E}$ ) is located in the northern part of the basin, at an altitude of 4350 m a.s.l. The lake is blocked by the lateral moraine of the Satopanth glacier toward the north. Hydrodynamic simulations are performed along the channel, from the Satopanth lake to the HEP located at Lam-bagarh, Vishnuprayag. The distance from the lake to the HEP stretches for about 28 km along the main flow channel. The flow channel has a hummocky surface due to the presence of thick debris for ~6–8 km from the lake to the headwater of the Alaknanda river. The channel takes a turn toward south from Mana village and flows downstream for 11 km until reaches the dam site. The channel is characterized by steep slopes and varied land use land cover (LULC). Figure 1 shows the study area; marked is the location of the lake and the hydropower dam.

### 3 Data used

#### 3.1 Satellite data

The present study exploits Landsat OLI/TIRS (30 m) of May 22, 2013 (LC08\_L1TP\_14 5039\_20130522\_20170504\_01\_T1), to map the lake extent prior to the cloudburst event that occurred on June 16–17, 2013 (Ray et al. 2016). Since no cloud-free Landsat satellite scene was available immediately after the cloudburst event, the lake area has been mapped from Raj and Kumar (2016) for June 21, 2013 (post-cloudburst). Terrain data for GLOF

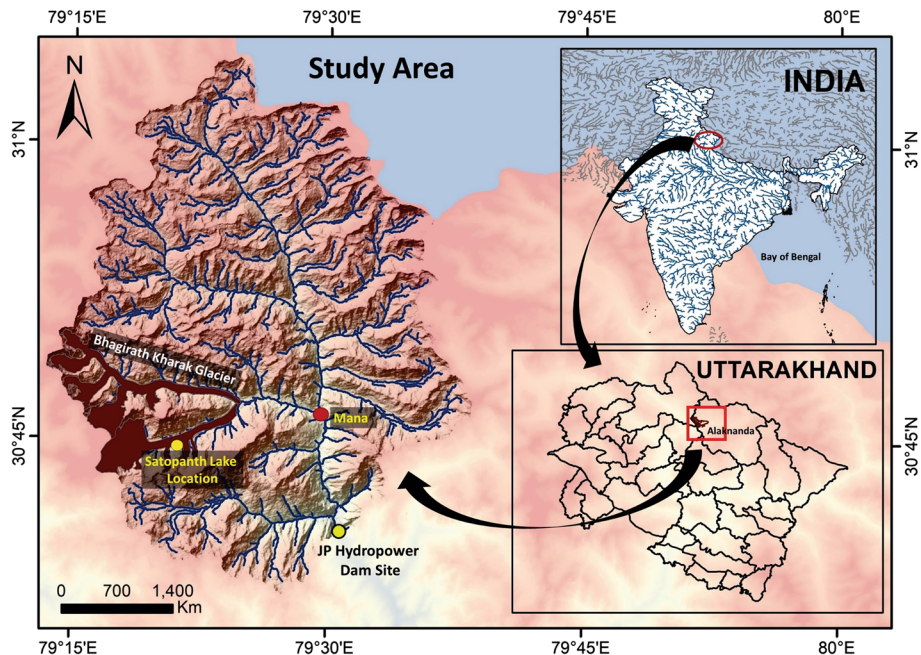


**Fig. 1** Map showing the location of the Alaknanda basin in the state of Uttarakhand, Central Himalaya; the location of the Satopanth lake, the Mana village and the hydropower dam site is shown in the given catchment

modeling have been obtained from the Advanced Spaceborne Thermal Emission and Reflection Radiometer (ASTER) global digital elevation model (GDEM). ASTER global DEM is a freely available model (<https://earthexplorer.usgs.gov/>) that provides elevation information between 83°N and 83°S with a spatial resolution of 30 m. A glacial lake inventory is prepared using Landsat OLI/TIRS (LC81450392015276LGN00) and cross-verified using high-resolution geo-referenced CNES/Airbus imagery tiles of Google earth. The land use land cover (LULC) classification, to determine Manning's roughness coefficient of the given terrain, is obtained using GlobCover (v2). GlobCover is the global product of land cover maps created from the 300 m MERIS sensor onboard of the ENVISAT satellite. The LULC (GlobCover) for the study area is further compared to the Landsat TM (LT05\_L1TP\_145039\_20101106\_20161012\_01\_T1) LULC map.

### 3.2 Field data

A total of over 1000 very high-resolution differential GPS (DGPS) points (model Leica GS25) were collected to map the lake extent and moraine height. In addition to this, over 900 points collected along the given valley were used to validate the LULC derived from satellite data. The acquired DGPS points displayed positional accuracy of < 1 cm. The 100-year return period flood data were collected from the dam site during the field visit (September 2017). Other relevant data of dam dimensions, flood marks and water discharge are obtained from the JP dam site at Lambagarh, Uttarakhand.

## 4 Methods

### 4.1 Inventory of glacial lakes and hydropower stations and temporal growth assessment of the Satopanth lake, Alaknanda basin

To evaluate the vulnerability of the 400 MW JP Vishnuprayag hydropower dam to a potential failure event of an existing lake located in the Alaknanda basin, an inventory of high-altitude lakes and hydropower dam is prepared. The proglacial, blocked and moraine-dammed lakes (Raj and Kumar 2016) more than 0.01 km<sup>2</sup> were considered for the inventory. The lakes were identified and mapped using Landsat OLI-derived Normalized Difference Water Index (NDWI). The formula used to derive NDWI (Huggel et al. 2002) is given in Eq. 1, where band 3 and band 5 are green and NIR channels, respectively. The locations and the extent of the lakes have been verified using high-resolution Google earth images. A total of 25 such lakes have been identified in the basin.

$$\text{NDWI} = \frac{\text{Band 3} - \text{Band 5}}{\text{Band 3} + \text{Band 5}} \quad (1)$$

Based on the data available from the Alternate Hydro Energy Centre (AHEC) for the different hydropower stations in the given basin, a GIS-based inventory is prepared. The stations are divided into three categories as: (1) stations in operation, (2) under construction and (3) proposed stations (Fig. 2).

A stream ordering of the basin is performed by applying the standard Arc Hydro tools on ASTER GDEM (Maidment and Morehouse 2002). The streams of the basin are categorized into six orders based on Strahler method of stream ordering (Shreve 1966). A GIS-based overlay operation reveals that all the HEP (in operation) are situated over the

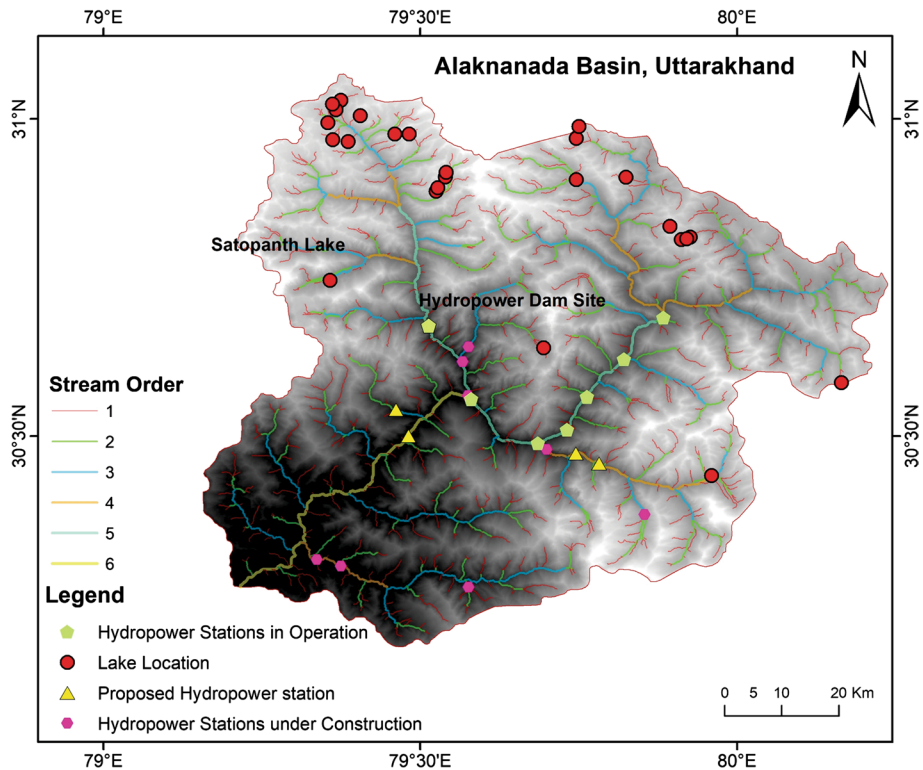


**Fig. 2** The Alaknanda basin showing the locations of the lakes and the hydropower stations (in operation, under construction and proposed); the drainage of the basin is divided into six stream orders

two main fifth-order streams, namely the Alaknanda and the Dhauliganga. Figure 2 shows the locations of the lakes, the hydropower stations and the drainage of the given basin. A proximity analysis indicated that the nearest lake to the 400 MW Vishnuprayag HEP is the Satopanth lake, which is located at a distance of 28 km upstream of the lake. As the Satopanth lake has been reported to be potentially hazardous (Worni et al. 2012), we perform a growth assessment of the lake using remote sensing imageries. We mapped the lake extent using satellite images of May 22, 2013 (pre-cloudburst), and June 21, 2013 (post-cloudburst) (Raj and Kumar 2016). The assessment reveals a significant increase in the size of the lake immediately after the cloudburst event. Figure 3 shows the pre- and post-cloudburst images of Satopanth lake. The total area of the lake before the cloudburst event was calculated to be 23834.8 m<sup>2</sup> as on May 22, 2013, which increased to 42246 m<sup>2</sup> after the event (Fig. 3a). A grown Satopanth lake mapped immediately after the cloudburst event is shown in Fig. 3b.

## 4.2 Field methods

The field methods in the present study involved (1) mapping of the Satopanth lake and the associated moraines, (2) collection of very high-resolution DGPS points along the given valley and (3) geotagging field photographs for the validation of LULC.

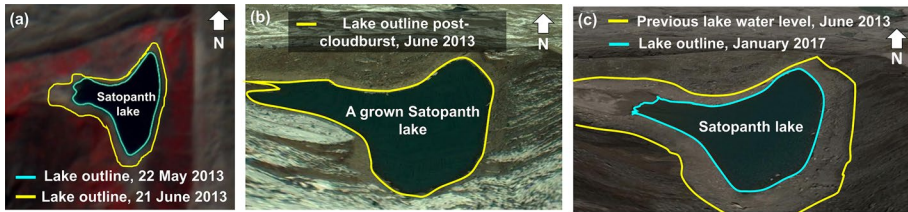


**Fig. 3** **a** Outline of the Satopanth lake mapped on May 2013 (pre-cloudburst) and June 2013 (post-cloudburst) (Raj and Kumar 2016); **b** a grown Satopanth lake after the cloudburst event, June 2013; **c** lake outlines mapped for the year 2017; the previous lake water level is marked in yellow

The DGPS points were collected using a Leica GS25 receiver, equipped with an inbuilt radio modem for higher accuracy. The points were collected using RTK (real-time kinematic) survey mode. The ability to measure a larger number of points in limited time is a major advantage of RTK surveys. In order to check the precision of the collected points, we selected 10 pilot ground points, where measurements were repeated thirty times for each point location. The DGPS repetitions over the given points revealed that the average horizontal accuracy of 1–3 cm and vertical of 2–5 cm remain constant for the first ten, twenty and thirty points and it further remains constant for even a single point. A total of over 1000 points covering an altitude range from 2242 m to 4321 m a.s.l have been collected.

#### 4.2.1 Lake and moraine mapping

A total of over 1000 points with an accuracy of < 1 cm were collected along the Satopanth lake boundary and the associated moraine. A DGPS base station is set at an elevated ground (moraine) as shown in Fig. 4c. We used a GPS receiver (rover) to measure point locations along the lake boundary and the moraine. Figure 4a shows the DGPS rover track along which the lake and the associated moraine were mapped. The freeboard of the lake is calculated using the difference in elevation points along the lake boundary and the crest of the associated moraine (Fig. 4b).

#### 4.2.2 LULC classification and validation

The land use land cover (LULC) map for the study region was first generated using multispectral Landsat TM (30 m). The satellite dataset chosen for the purpose was such that (1) it covers the entire valley of interest, from the Satopanth lake to the HEP (2) and has < 10% cloud cover. The Gaussian maximum likelihood (GML) algorithm is applied to the satellite data for classification. The GML is a robust method of classification (Chen et al. 2004) which efficiently classifies the given image by considering mean, variances and covariance of the training samples. The classification resulted in a total of six LULC categories. The Landsat LULC is compared to the Envisat Meris-derived ESA GlobCover LULC (version 2.3) (Bontemps et al. 2011). It is evident that GlobCover is a more reliable source to obtain LULC classified data for the given region, as it categorizes the region into a total of eleven classes. The LULC (GlobCover) is extracted for a buffer zone of 250 m around the main flow channel, in a way that it also covers the flood plains of the given channel. In order to validate the derived LULC (GlobCover), a set of high-resolution DGPS sample points were collected in the field at different

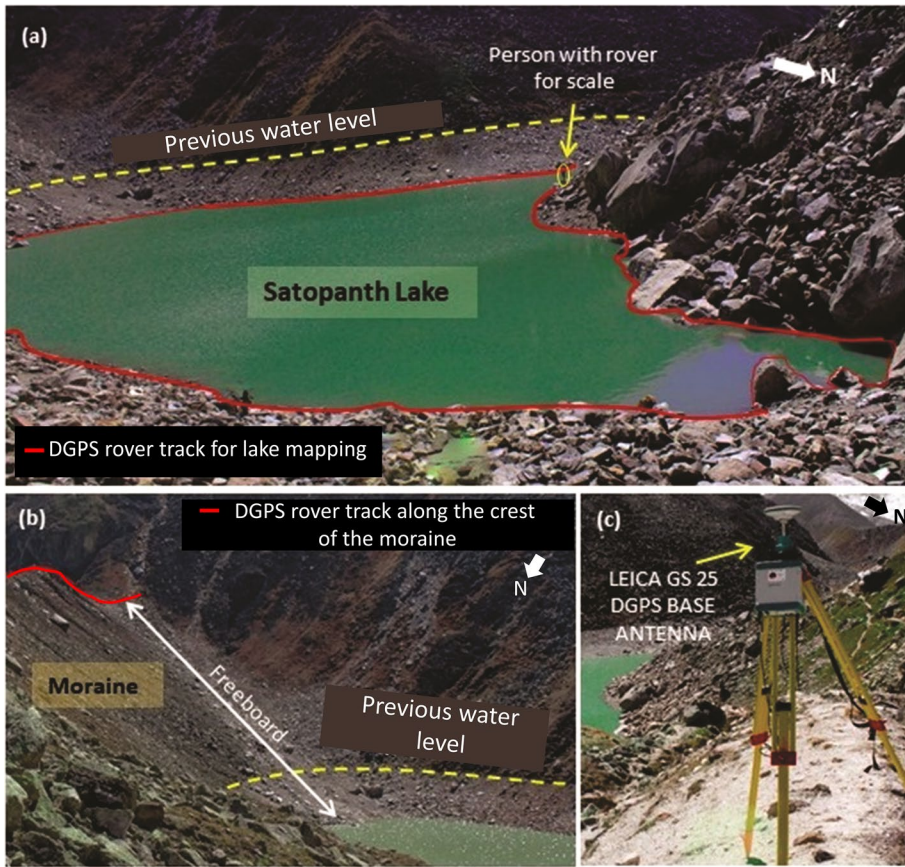


**Fig. 4** **a** Satopanth lake showing the DGPS rover track (person with rover for scale); **b** rover track along the crest of the lateral moraine; **c** location of the DGPS base station set at a higher elevation

locations over different LULC ground classes. To validate the same for the inaccessible areas, geotagged field photographs were taken at different locations along the main flow channel. Figure 5 shows the spatial distribution of LULC along the buffer zone of the main flow channel and the DGPS point locations for LULC validation.

The Manning's roughness coefficient defines the frictional resistance of a terrain exerted on given flow (Coon 1998). The values of Manning's roughness coefficient are assigned based on the ground conditions that exist at the time of a particular flow event (Carter et al. 1963; Arcement et al. 1989). In the present study, we derive the Manning's  $N$  along the flow channel from the Satopanth lake to the HEP using the extracted LULC. We assume that the LULC of the given area has not changed much over the years. Table 1 shows the LULC classes of the study area with their respective Manning's roughness coefficient and the ground validation points. It is evident that more than 90% of the flow area has LULC classes with Manning's  $N$  ranging from 0.034 to 0.06. A Manning's  $N$  in the range from 0.04 to 0.06 has mostly been used for hydrodynamic simulation for Himalayan rivers (Worni et al. 2012; Jain et al. 2012;



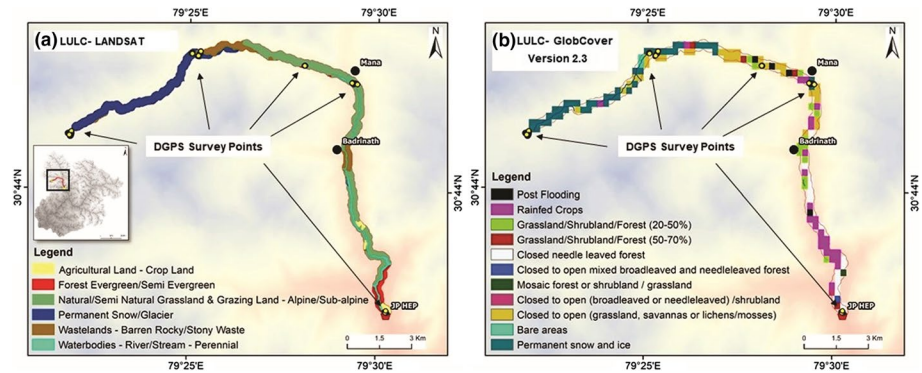


**Fig. 5** LULC extracted for the buffer zone along the main flow channel derived using **a** Landsat TM; **b** LULC GlobCover (Version 2.3); yellow dots show the DGPS points for validation

Thakur et al. 2016). In the present study, we consider the average of all the Manning’s roughness coefficient values ( $N = 0.045$ ) present along the given channel.

### 4.3 GLOF modeling and flood routing coupled with a 100-year return period flood event

In the present study, we perform both one-dimensional and two-dimensional computations of the flow hydraulics in a potential GLOF event of the Satopanth lake combined with a 100-year return period flood. The one-dimensional hydrodynamic models are based on the Saint-Venant’s or shallow water equations (SWE) where conservation of mass and momentum is taken into consideration along a single direction (Brunner 2002). On the other hand, two-dimensional models solve SWE, to produce depth-averaged and spatially distributed hydraulic characteristics of a given flow (Chanson 2004).

The total volume of water released during a GLOF event is one of the prime inputs for hydrodynamic models in order to simulate a moraine-breach event (Westoby et al. 2014). Since no ground estimate of the total water volume of the lake is available, an empirical relation by Huggel et al. (2002) is used to calculate the total volume of the Satopanth lake. The equation is given as follows:

$$V = 0.104A^{1.42} \tag{2}$$

where  $V$  is the total volume of the lake and  $A$  is the total surface area of the lake. The aerial extent of the lake, immediately after the 2013 cloudburst event, has been considered to calculate the volume. The total area of the Satopanth lake as on June 21, 2013, was calculated to be  $42246 \text{ m}^2$  (Raj and Kumar 2016). The volume thus calculated using Eq. 2 is  $3.85 \times 10^5 \text{ m}^3$ . Other model input parameters for dynamic modeling of GLOF include Manning’s roughness coefficient, river reach, channel bank lines, valley cross sections and breach formation time. The river reach, channel bank lines and valley cross sections are derived using GIS-based operations on ASTER GDEM and high-resolution Google earth images.

**Table 1** LULC classes of the study area with their respective Manning's *N* roughness coefficient and DGPS point locations for validation

LULC Class	Manning's <i>N</i>	Validation location (Lat/Long)	DGPS/Geotagged field photographs (GFP)
Permanent snow and ice	0.04	30°44'44.39"N 79°21'46.40"E	DGPS and GFP
Bare areas	0.035	–	–
Closed to open (grassland, savannas or lichens/mosses)	0.034	30°47'00.78"N 79°26'51.11"E	DGPS and GFP
Closed to open (broad-leaved or needle-leaved forest)/shrub land	0.05	30°43'13.69"N 79°29'44.90"E	GFP
Mosaic forest or shrub land/grassland	0.034	–	–
Closed to open mixed broad-leaved and needle-leaved forest	0.035	–	–
Closed needle-leaved forest	0.11	30°41'48.58"N 79°30'36.13"E	GFP
Grassland/shrub land/forest (50–70%)	0.034	30°46'39.26"N 79°28'15.93"E	DGPS and GFP
Grassland/shrub land/forest (20–50%)	0.035	30°46'39.77"N 79°28'24.63"E	GFP
Rainfed crops	0.06	–	–
Post-flooding	0.03	30°46'37.60"N 79°28'22.39"E	DGPS and GFP

### 4.3.1 Distribution of 100-year return period flood

A 100-year return period flood is a flood event that has a 1% probability of occurring in any given year (Chow et al. 1988). Thus, it very crucial to analyze severe combinations of GLOF events and extreme floods (100-year return period event) which may arise due to critical meteorological conditions in a given region. In the present study, we initially evaluate the 100-year return period flood distribution in the given basin. Further, we combine the 100-year flood discharge with the potential GLOF discharge and study its effect on the hydraulic properties of the potential flood wave. The 100-year return period flood data ( $2200 \text{ m}^3\text{s}^{-1}$  at the dam site) were collected from the HEP dam authorities (Jaypee) during the field visit.

In order to distribute the 100-year flood discharge at a sub-catchment level, we employed ASTER GDEM to delineate the major and the minor watersheds. The Arc Hydro tools (Arc Map 10.3) have been exploited to perform necessary hydrological operations. Primarily, the major watershed is delineated by taking an outlet discharge point at the JP HEP dam site. This is further divided into six sub-catchments using different discharge points along the main flow channel, as shown in Fig. 6. The 100-year

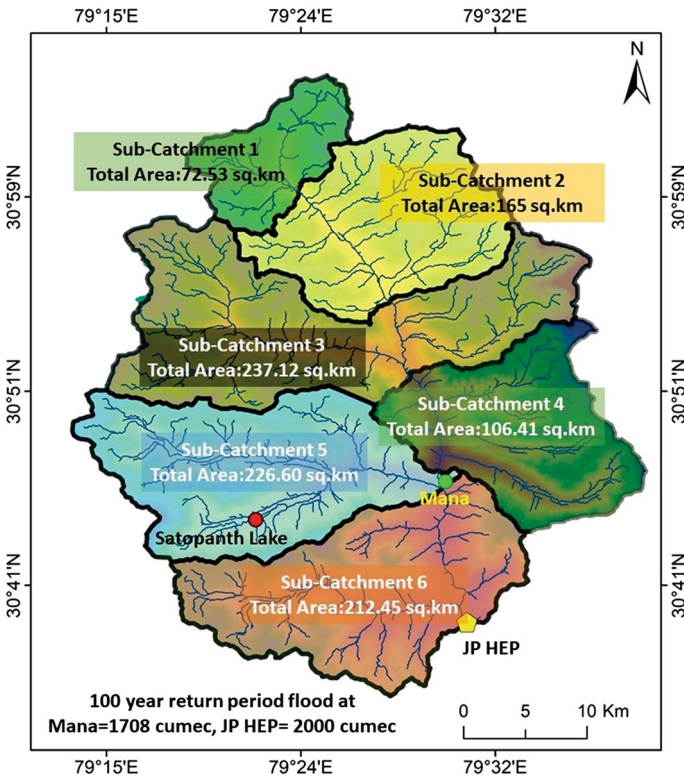


**Fig. 6** Total catchment of the JP HEP divided into six sub-catchments based on different outlet discharge points along the main flow channel; the 100-year return period flood at Mana village is calculated to be  $\sim 1700 \text{ m}^3\text{s}^{-1}$

flood is distributed based on the total area of the sub-watersheds using Dickens formula (1865) (Alexander 1972). It is given by the equation:

$$Q_p = C_D A^{\frac{3}{4}} \quad (3)$$

where  $Q_p$  is the maximum flood discharge in  $\text{m}^3\text{s}^{-1}$ ,  $A$  is the catchment area in  $\text{km}^2$  and  $C_D$  is Dickens constant which has a value of 11 to 14 for northern Indian hilly regions. In the present study,  $C_D$  is calculated to be 11.1 based on the total area of the major catchment. The entire area of the major catchment is calculated to be  $1020 \text{ km}^2$ . The 100-year return period flood discharge at Mana village is calculated to be  $\sim 1700 \text{ m}^3\text{s}^{-1}$  (Eq. 3). In the present study, the potential GLOF discharge of the Satopanth lake is coupled with the 100-year return flood discharge at Mana village and the combined effect of the flood event is analyzed till it reaches the dam site located further downstream.

#### 4.3.2 One-dimensional GLOF modeling and flood routing combined with 100-return period flood

In the present study, we employ the HEC-RAS 1D hydrodynamic model (Brunner 2002) to simulate a moraine-breach event of the Satopanth lake. The HEC-RAS model is one of the most popular open source models used for glacial hazard studies (Alho et al. 2005; Alho and Juha 2008; Carling et al. 2010). Here, we model a potential moraine-failure event that releases the total volume of the lake. It is assumed that the total width of the moraine fails (dimensions derived from DEM) in order to release the stored volume of the lake. A set of different moraine-failure times (0.5 h, 0.7 h and 1.0 h) has been used to calculate the initial breach hydrograph. The hydrograph that produced the maximum peak flood (worst-case scenario) is routed along the main flow channel until it reaches the HEP dam site. The cross sections of the main flow channel were derived (ASTER DEM) for every 500 m along the full length of the channel in a way that they cover the entire floodplain. Figure 7 shows the plot of the

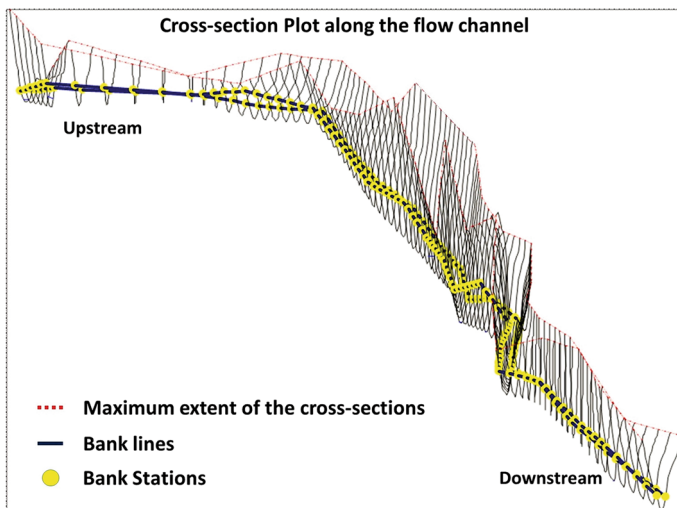


**Fig. 7** Plot of the DEM-derived cross sections along the main flow channel; the maximum mapped extent and the bank stations along the given channel are shown in red and yellow, respectively

DEM-derived cross sections along the main flow channel. The central axis of the main flow channel (flow path) and the maximum flood extent (bank lines) are delineated using high-resolution Google earth images.

In the routing process, breach hydrograph and the frictional slope between the last two cross sections are taken as the upstream and downstream boundary condition, respectively (Brunner 2010). The flood hydrographs were evaluated at different locations along the flow channel to determine the amount and the time of peak discharge. The resultant hydrograph is then coupled with the calculated 100-year flood discharge (Sect. 4.3.1) at Mana village and further routed until it reaches the hydropower dam site. An average Manning's roughness coefficient of 0.045 as calculated in Sect. 4.2.2 has been considered.

### 4.3.3 Two-dimensional GLOF modeling and flood routing combined with a 100-year return period flood

A two-dimensional unsteady flow modeling of a potential Satopanth lake GLOF event is performed using the latest version of HEC-RAS (v 5.0.5), which delivers an effective solution for Saint-Venant's equations in a 2D array. The two-dimensional modeling routes the initial breach hydrograph over a raster-based terrain. In the present study, the terrain is divided into a mesh with equal grid dimensions of 30×30. Each cell is defined with a set of terrain properties like Manning's roughness coefficient and elevation. The projection system of UTM 44 has been defined based on the location of the present study. A 2D flow area is initially defined within the limits of the terrain model containing the lake and the HEP. A Manning's  $N$  of 0.045 (Sect. 4.2.2) is assigned to each cell within the 2D flow area. The upstream and downstream boundary conditions are the same as one-dimensional modeling (Sect. 4.3.2). Unsteady hydraulic routing of the breach hydrograph is performed for a distance of 28 km from the lake until it reaches the HEP. In the hydraulic routing process, we combine the calculated 100-year flood discharge (Sect. 4.3.1) with the potential GLOF discharge at Mana village and study its effect on the hydraulic properties of the potential flood wave. A temporal assessment of the spatially distributed outputs of water depth, velocity and inundation of a GLOF event coupled with a 100-year return period flood of the catchment is performed at the dam site. In addition, we also perform the 2D hydraulic computation of stream power for the potential flood wave. The stream power is the product of the average flow velocity and the average shear stress. The shear stress is given by the equation:

$$\tau = \rho g dS \quad (4)$$

where  $\tau$  is the shear stress in  $\text{N m}^{-2}$ ,  $\rho$  is the specific density of water in  $\text{kg m}^{-3}$ ,  $g$  is acceleration due to gravity in  $\text{ms}^{-1}$  and  $S$  is the energy gradient calculated from the channel slope. Temporal evaluation of the 2D hydraulic properties of the potential flood wave at the dam site is performed. The 2D outputs of the modeled flood event were mapped at two different time steps: first, when the flood wave arrives at the dam site and second, at the initiation of the dam overflow. Figure 8 shows the overall methodology of the present study.

## 5 Results and discussion

The Satopanth lake is identified as one of the potentially critical lakes located in the Alaknanda basin, Central Himalaya (Worni et al. 2012). Here, we performed one-dimensional and two-dimensional hydraulic modeling of a potential GLOF of the lake and evaluated its impact on a

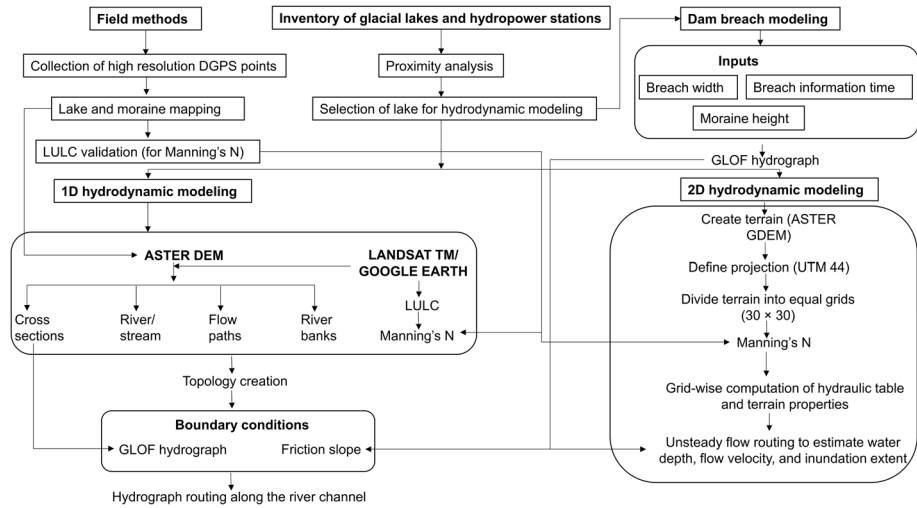


**Fig. 8** Flowchart showing the methodology of one-dimensional and two-dimensional GLOF modeling for Satopanth lake, Alaknanda basin

HEP located downstream. A moraine-breach modeling releasing the total volume of the lake was performed for different failure times of 0.5 h, 0.7 h and 1.0 h. The total lake volume calculated immediately after the 2013 cloudburst event ( $3.8 \times 10^5 \text{ m}^3$ ) has been considered for its hazard assessment. Figure 9a shows the modeled GLOF hydrographs for different failure times. In order to evaluate the worst-case GLOF scenario, we performed one-dimensional hydraulic routing of the breach hydrograph with a peak discharge of  $870 \text{ m}^3\text{s}^{-1}$ , produced in a breach formation time of 0.5 h. The routing was carried out for a distance of 28 km along the main flow channel from the Satopanth lake to the dam site. It is assumed that the major attenuation ( $\sim 30\%$ ) of the peak flood occurs within the initial 6–8 km due to the hummocky surface of the flow area. We evaluated the discharge hydrographs at different locations along the flow channel to determine the peak flood and the time of peak. A hydrograph with a peak discharge of  $315 \text{ m}^3\text{s}^{-1}$  is obtained at Mana village which is located at a distance of 16.5 km downstream of the lake (Fig. 9b). The flood was further routed until it reaches the dam site coupled with the discharge of a 100-year return period flood discharge of  $\sim 1700 \text{ m}^3\text{s}^{-1}$  at Mana village (Sect. 4.3.1). The average Manning’s *N* of 0.045 based on the LULC has been considered in the present study (Sect. 4.2.2). A sensitivity analysis of the model to the average Manning’s *N*

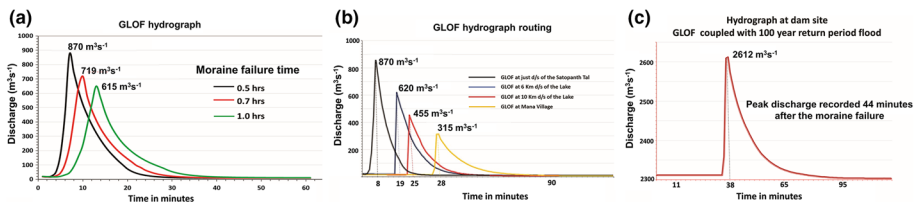


**Fig. 9** a Breach hydrographs for different moraine-failure times of 0.5 h, 0.7 h and 1.0 h; b GLOF hydrograph at different locations along the flow channel; c GLOF hydrograph coupled with a 100-year flood at the dam site

for the study area shows a variation of 5 to 6 percent in the peak discharge when  $n$  is 0.01. The flood wave arrives at the HEP dam site 38 min after the initiation of the failure event, producing a flood with a peak discharge of  $\sim 2600 \text{ m}^3\text{s}^{-1}$ . Figure 9c shows the routed flood hydrograph at the dam site produced during the combination of GLOF and the 100-year flood discharge.

Two-dimensional hydraulic GLOF routing was carried out using the same set of boundary conditions and input parameters as that in the one-dimensional model. Flow simulations to analyze the hydraulic behavior of a potential GLOF wave were performed over a 2D gridded terrain. The routed GLOF discharge is combined with the 100-year flood discharge at Mana village. The lowermost cross section nearest to the HEP is considered as the dam structure and is assumed that the control gates of the dam remain closed. The Satopanth GLOF coupled with 100-year flood resulted in a potential flood wave that arrives at the dam site at a maximum flow velocity of  $7.6 \text{ ms}^{-1}$ . A maximum inundation depth of 7.2 m is reached at the dam site immediately after the flood wave arrival. The stream power is calculated taking into consideration the shear stress as given in Sect. 4.3.3. The stream power being a function of flow velocity, a gradual decrease in the stream power at the dam site is evident as the flow velocity decreases. Figure 10a, b shows the spatially distributed plots of flow velocity, stream power, inundation depth and extent derived using 2D hydraulic routing.

The data of dam height and crest length were obtained during the field visit, which are 17 m and 63 m, respectively. The temporal evaluation of the 2D modeled hydraulic outputs at the dam site shows a rapid increase in the water depth at an average rate of 4.5 m per minute. At this rate, the maximum height of the dam is reached within 4 min after the initial flood wave arrival, leading to a dam overflow. In addition, flood inundation extent is mapped at the time of dam overflow, i.e., 4 min after the initial flood wave arrival. The modeled flood inundation width of the potential flood obtained at the dam site is 136 m, which is 73 m more than the dam crest length. This implies that the flood water would potentially inundate the area surrounding the dam.

The results produced in the present study can be compared to the 2013 cloudburst event (Dobhal et al. 2013; Ray et al. 2016) that impacted this dam located at Vishnuprayag, leading to overflow and causing great damage to the dam infrastructure and also in the downslope regions. A discharge of  $\sim 2200 \text{ m}^3\text{s}^{-1}$  was recorded at the dam site during the 2013 event (data from the HEP dam authorities). Figure 11a shows a photograph of the dam site during the 2013 flood. A field photograph taken during field visit (September 2017) shows the previous flood marks at a distance of 100 m upstream of the dam site (Fig. 11b). The results of the present study reveal that a potential discharge of  $\sim 2600 \text{ m}^3\text{s}^{-1}$  at the dam site, which is  $\sim 400 \text{ m}^3\text{s}^{-1}$  in excess than what was caused in 2013, would lead to a more severe flood situation. Therefore, considering glacial lake outburst flood assessment of the Satopanth lake was crucial to evaluate the vulnerability of the JP HEP to the severe flood situation, as sudden discharge from the high-altitude lakes can amplify an existing flood situation.

## 6 Conclusion

The Satopanth lake is not only reported to be one of the potentially critical lakes in the available literature (Worni et al. 2012) but also has past evidence of lake-level changes due to cloudburst events in the higher reaches of the basin. The present study evaluated the hazard potential of the Satopanth lake when combined with a 100-year return period flood event. Further, its impact on a HEP located at a distance of 28 km downstream is assessed

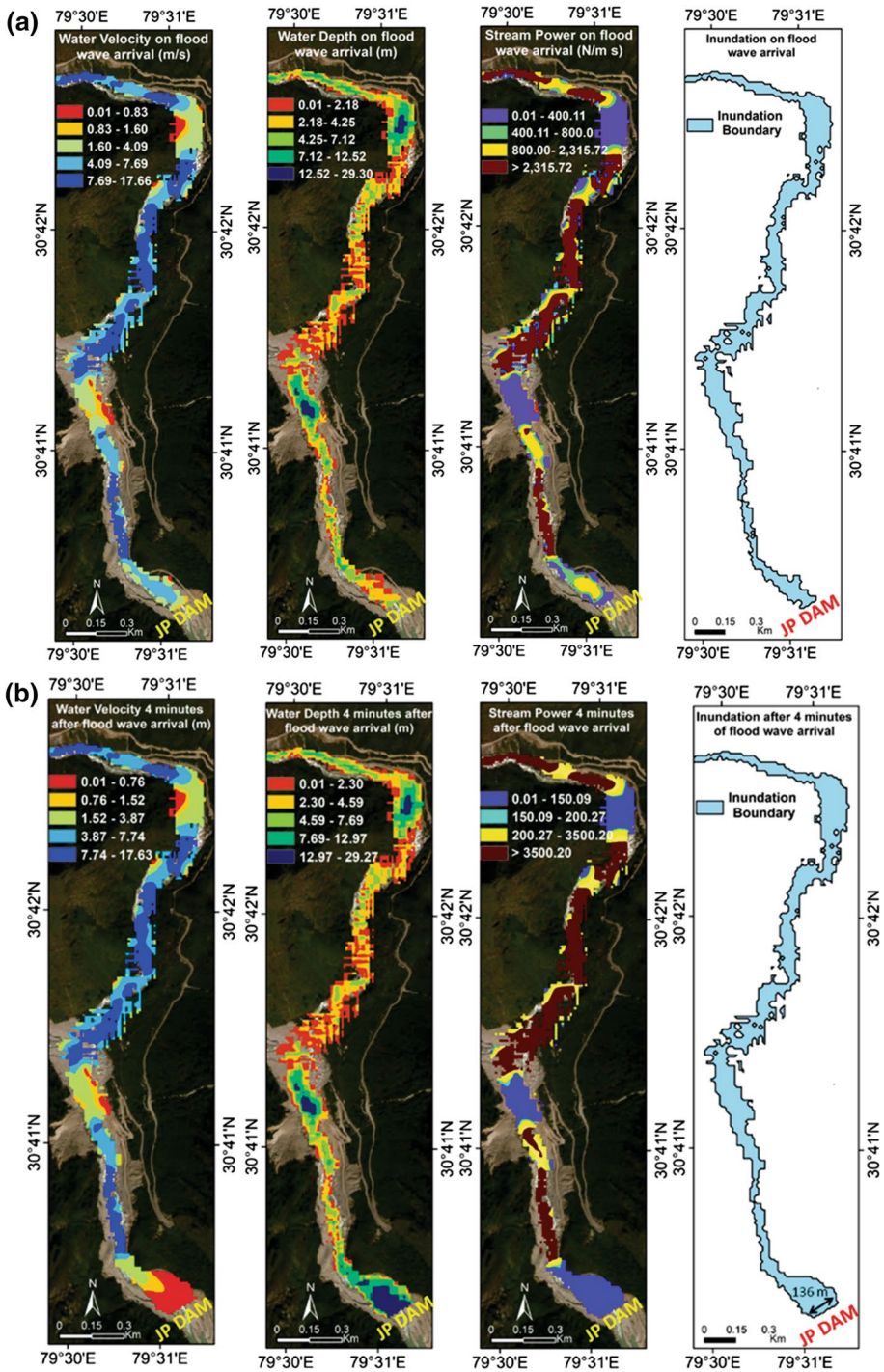


**Fig. 10** a 2D plots of flow velocity, water depth, stream power and inundation extent immediately after the flood wave arrival. b 2D plots of flow velocity, water depth, stream power and inundation extent, 4 min after the flood wave arrival



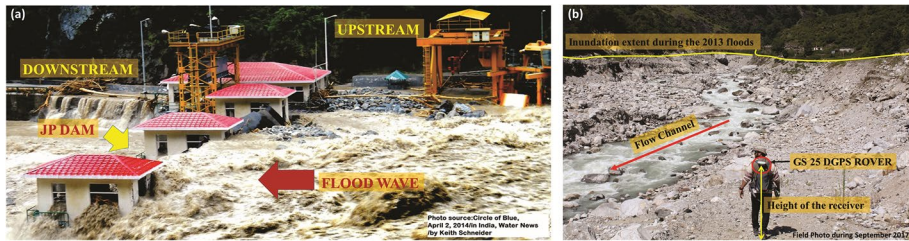


**Fig. 11** **a** JP dam site during the 2013 floods with the discharge with  $\sim 2200 \text{ m}^3\text{s}^{-1}$ . **b** Field photograph at 100 m upstream of the dam site showing the 2013 flood inundation marks along the flow channel

using 1D and 2D hydrodynamic models. A series of moraine-breach events of the lake were modeled to calculate the discharge for different moraine-failure scenarios. Considering the lake volume, the GLOF discharge even in a worst-case scenario is not significant to cause any damage to the downstream region; however, when combined with an extreme flood event, it has a significant impact on the hydropower station located downstream.

The GLOF modeling of the Satopanth lake coupled with a 100-year return period flood resulted in a peak discharge of  $\sim 2600 \text{ m}^3\text{s}^{-1}$  at the dam site that would potentially inundate the dam infrastructure. The potential GLOF wave arrived at the dam site 38 min after the initiation of the moraine-breach event. Two-dimensional routing of the GLOF hydrograph was performed from the lake to the dam site to evaluate the spatially distributed hydraulic properties of the potential flood wave. The potential GLOF wave when combined with the 100-year return period discharge at Mana village resulted in a flood that arrived at the dam site with a velocity of  $7.6 \text{ ms}^{-1}$ . Assuming that the control gates of the dam remain closed, the water depth at the dam site increases at a rate of 4.5 m per minute. The dam overflows at approximately 4 min after the initial arrival of the flood wave. The unavailability of high-resolution terrain data limits the degree of accuracy in the computation of the hydraulic properties of the potential flood. The study recommends regular monitoring of the Satopanth lake especially during post-monsoon season, due to the potential risk it imposes on the downstream region when combined with high-intensity precipitation events.

**Acknowledgements** The authors would like to acknowledge the Indian Institute of Technology, Roorkee, India, for providing necessary infrastructure facilities. The authors also acknowledge the MHRD, MoES (IMPRINT) and DST INSPIRE fellowship for providing the necessary financial support. We are grateful to the JP group for providing relevant data to carry out the work. We thank USGS for the free satellite products employed in the study.

## References

- Ageta Y, Iwata S, Yabuki H et al (2000) Expansion of glacier lakes in recent decades in the Bhutan Himalayas. *IAHS Publ* 264:165–175
- Alexander GN (1972) Effect of catchment area on flood magnitude. *J Hydrol* 16:225–240. [https://doi.org/10.1016/0022-1694\(72\)90054-6](https://doi.org/10.1016/0022-1694(72)90054-6)
- Alho P, Juha A (2008) Comparing a 1D hydraulic model with a 2D hydraulic model for the simulation of extreme glacial outburst floods. *Hydrol Process Int J* 22(10):1537–1547. <https://doi.org/10.1002/hyp.6692>
- Alho P, Russell AJ, Carrivick JL, Käyhkö J (2005) Reconstruction of the largest Holocene jökulhlaup within Jökulsá á Fjöllum, NE Iceland. *Quat Sci Rev* 24(22):2319–2334. <https://doi.org/10.1016/j.quascirev.2004.11.021>

- Allen SK, Rastner P, Arora M, Huggel C, Stoffel M (2016) Lake outburst and debris flow disaster at Kedarnath, June 2013: hydrometeorological triggering and topographic predisposition. *Landslides* 13(6):1479–1491
- Arcement, George J, Verne R Schneider (1989) Guide for selecting Manning's roughness coefficients for natural channels and flood plains. Water-supply paper/United States Geological Survey, 2339
- Bolch T, Kulkarni A, Kaab A, Huggel C, Paul F, Cogley JG, Frey H, Kargel JS, Fujita K, Scheel M et al (2012) The state and fate of Himalayan glaciers. *Science* 336(6079):310–314. <https://doi.org/10.1126/science.1215828>
- Bontemps S, Defourny P, Bogaert EV, Arino O, Kalogirou V, Perez JR (2011) GLOBCOVER 2009-Products description and validation report
- Bookhagen B, Burbank DW (2006) Topography, relief, and TRMM-derived rainfall variations along the Himalaya. *Geophys Res Lett* 33:1–5. <https://doi.org/10.1029/2006GL026037>
- Brunner GW (2002) HEC-RAS, river analysis system, hydraulic reference manual. Hydrologic Engineering Center, US Army Corps of Engineers, Davis
- Brunner GW (2010) HEC-RAS River analysis system hydraulic reference manual. U.S. Army Corps of Engineers Hydrologic Engineering Center (HEC), 411
- Carey M (2005) Living and dying with glaciers : people's historical vulnerability to avalanches and outburst floods in Peru. *Glob Planet Change B* 47:122–134. <https://doi.org/10.1016/j.gloplacha.2004.10.007>
- Carling P, Villanueva I, Herget J, Wright N, Borodavko P, Morvan H (2010) Unsteady 1D and 2D hydraulic models with ice dam break for Quaternary megaflood, Altai Mountains, southern Siberia. *Global Planet Change* 70(1–4):24–34. <https://doi.org/10.1016/j.gloplacha.2009.11.005>
- Carter RW, Einstein HA, Hinds J, Powell RW, Silberman E (1963) Friction factors in open channels, progress report of the task force on friction factors in open channels of the Committee on Hydro-mechanics of the Hydraulics Division. *Proc Am Soc Civ Eng J Hydraul Div* 89:97–143
- Chanson H (2004) *Hydraulics of open channel flow*. Elsevier, Amsterdam
- Chen D, Stow DA, Gong P (2004) Examining the effect of spatial resolution and texture window size on classification accuracy: an urban environment case. *Int J Remote Sens* 25(11):2177–2192. <https://doi.org/10.1080/01431160310001618464>
- Chow VT, Maidment DR, Mays LW (1988) *Applied hydrology*. McGraw-Hill, New York, p 572
- Clague JJ, Evans SG (2000) A review of catastrophic drainage of moraine-dammed lakes in British Columbia. *Quatern Sci Rev* 19(17–18):1763–1783. [https://doi.org/10.1016/S0277-3791\(00\)00090-1](https://doi.org/10.1016/S0277-3791(00)00090-1)
- Coon WF (1998) Estimation of roughness coefficients for natural stream channels with vegetated banks (Vol 2441). US Geological Survey
- Das PK (2013) The Himalayan Tsunami—Cloudburst, Flash flood & death toll : a. The Himalayan Tsunami—cloudburst, flash flood & death toll : a geographical postmortem (June). <https://doi.org/10.9790/2402-0723345>
- Dobhal DP, Gupta AK, Mehta M, Khandelwal DD (2013) Kedarnath disaster: facts and plausible causes. *Curr Sci* 105(2):171–174
- Emmer A (2018) GLOFs in the WOS: Bibliometrics, geographies and global trends of research on glacial lake outburst floods (Web of Science, 1979–2016). *Nat Hazards Earth Sys Sci* 18(3):813–827
- Gardelle J, Arnaud Y, Berthier E (2011) Contrasted evolution of glacial lakes along the Hindu Kush Himalaya mountain range between 1990 and 2009. *Global Planet Change* 75(1–2):47–55. <https://doi.org/10.1016/j.gloplacha.2010.10.003>
- Ghosh S, Lunija V, Gupta A (2009) Trend analysis of Indian summer monsoon rainfall at different spatial scales. *Atmos Sci Lett* 10(4):285–290. <https://doi.org/10.1002/asl.235>
- Haerberli W (1983) Frequency and characteristics of glacier floods in the Swiss Alps. *Ann Glaciol* 4:85–90
- Heeswijk M, Kimball JS, Marks DG (1996) Simulation of water available for runoff in clearcut forest openings during rain-on-snow events in the western cascade range of Oregon and Washington. In: USGS water-resources investigations report 954219, Tacoma, Washington, 67
- Huggel C, Kääb A, Haerberli W, Teyssie P, Paul F (2002) Remote sensing based assessment of hazards from glacier lake outbursts: a case study in the Swiss Alps. *Can Geotech J* 39(2):316–330. <https://doi.org/10.1139/t01-099>
- Ives JD, Shrestha RB, Mool PK (2010) Formation of Glacial Lakes in the Hindu Kush-Himalayas and GLOF risk assessment. ICIMOD (International Centre for Integrated Mountain Development), p 66
- Jain SK, Lohani AK, Singh RD, Chaudhary A, Thakural L (2012) Glacial lakes and glacial lake outburst flood in a Himalayan basin using remote sensing and GIS. *Nat Hazards* 62(3):887–899. <https://doi.org/10.1007/s11069-012-0120-x>
- Komori J (2008) Recent expansions of glacial lakes in the Bhutan Himalayas. *Quatern Int* 184(1):177–186. <https://doi.org/10.1016/j.quaint.2007.09.012>

- Kulkarni AV, Bahuguna IM, Rathore BP et al (2007) Glacial retreat in Himalaya using Indian remote sensing satellite data. *Curr Sci* 92:69–74. <https://doi.org/10.1117/12.694004>
- Lliboutry L, Arnao BM, Pautre A, Schneider B (1977) Glaciological problems set by the control of dangerous lakes in Cordillera Blanca, Peru I Historical failures of morainic dams, their causes and prevention. *J Glaciol* 18(79):239–254
- Maidment DR, Morehouse S (2002) Arc hydro: GIS for water resources. ESRI Inc, Redlands
- Mergili M, Schneider JF (2011) Regional-scale analysis of lake outburst hazards in the southwestern Pamir, Tajikistan, based on remote sensing and GIS. *Nat Hazards Earth Syst Sci* 11(5):1447–1462. <https://doi.org/10.5194/nhess-11-1447-2011>
- Mool PK, Wangda D, Bajracharya SR, Kunzang KARMA, Gurung DR, Joshi SP (2001) Inventory of glaciers, glacial lakes and glacial lake outburst floods. Monitoring and early warning systems in the Hindu Kush-Himalayan Region: Bhutan. Inventory of glaciers, glacial lakes and glacial lake outburst floods. Monitoring and early warning systems in the Hindu Kush-Himalayan Region: Bhutan. vol 227 pp. 49
- Nie Y, Liu Q, Liu S (2013) Glacial lake expansion in the Central Himalayas by Landsat images, 1990–2010. *PLoS ONE* 8(12):e83973
- Osti R, Egashira S (2009) Hydrodynamic characteristics of the Tam Pokhari Glacial Lake outburst flood in the Mt. Everest region, Nepal. *Hydrol Process Int J* 23(20):2943–2955. <https://doi.org/10.1002/hyp.7405>
- Pattanaik DR, Pai DS, Mukhopadhyay B (2015) Rapid northward progress of monsoon over India and associated heavy rainfall over Uttarakhand: a diagnostic study and real time extended range forecast. *Mausam* 66:551–568
- Quincey DJ et al (2007) Early recognition of glacial lake hazards in the Himalaya using remote sensing datasets. *Global Planet Change* 56:137–152. <https://doi.org/10.1016/j.gloplacha.2006.07.013>
- Raj KBG, Kumar KV (2016) Inventory of Glacial Lakes and its evolution in Uttarakhand Himalaya Using Time Series Satellite Data. *J Indian Soc Remote Sens* 44(6):959–976. <https://doi.org/10.1007/s12524-016-0560-y>
- Ray PC, Chatteraj SL, Bisht MPS, Kannaujiya S, Pandey K, Goswami A (2016) Kedarnath disaster 2013: causes and consequences using remote sensing inputs. *Nat Hazards* 81(1):227–243. <https://doi.org/10.1007/s11069-015-2076-0>
- Richardson SD, Reynolds JM (2000) An overview of glacial hazards in the Himalayas. *Quatern Int* 65–66:31–47. [https://doi.org/10.1016/S1040-6182\(99\)00035-X](https://doi.org/10.1016/S1040-6182(99)00035-X)
- Sattar A, Goswami A, Kulkarni AV (2019) Hydrodynamic moraine-breach modeling and outburst flood routing—a hazard assessment of the South Lhonak lake, Sikkim. *Sci Total Environ* 668:362–378. <https://doi.org/10.1016/j.scitotenv.2019.02.388>
- Shreve RL (1966) Statistical law of stream numbers. *J Geol* 74(1):17–37
- Stoffel M, Huggel C (2012) Effects of climate change on mass movements in mountain environments. *Prog Phys Geogr* 36(3):421–439. <https://doi.org/10.1177/0309133312441010>
- Thakur PK, Aggarwal S, Aggarwal SP, Jain SK (2016) One-dimensional hydrodynamic modeling of GLOF and impact on hydropower projects in Dhauliganga River using remote sensing and GIS applications. *Nat Hazards* 83(2):1057–1075. <https://doi.org/10.1007/s11069-016-2363-4>
- Wang W et al (2015) Rapid expansion of glacial lakes caused by climate and glacier retreat in the Central Himalayas. *Hydrol Process* 874:859–874. <https://doi.org/10.1002/hyp.10199>
- Westoby MJ, Glasser NF, Brasington J, Hambrey MJ, Quincey DJ, Reynolds JM (2014) Modelling outburst floods from moraine-dammed glacial lakes. *Earth Sci Rev* 134:137–159. <https://doi.org/10.1016/j.earscirev.2014.03.009>
- Worni R, Stoffel M, Huggel C, Volz C, Casteller A, Luckman B (2012) Analysis and dynamic modeling of a moraine failure and glacier lake outburst flood at Ventisquero Negro, Patagonian Andes (Argentina). *J Hydrol* 444–445:134–145. <https://doi.org/10.1016/j.jhydrol.2012.04.013>